JOURNAL OF AIRCRAFT
Vol. 34, No. 2, March–April 1997

Active Flutter Suppression Using Multi-Input/Multi-Output Adaptive Least Mean Square Control

Walter Eversman* and Indranil Danda Roy†
University of Missouri–Rolla, Rolla, Missouri 65401

The feasibility of an adaptive feedforward multi-input/multi-output (MIMO) controller for active flutter suppression has been investigated in this study. An unswept flexible wing structure is modeled by a multi-degree-of-freedom finite element representation with beam elements for bending and rod elements for torsion. Control action is provided by one or more flaps attached to the trailing edge of the wing and extending along a fraction of the wingspan. Time-domain unsteady aerodynamics have been used to generate the air forces acting on the wing model. The adaptive feedforward MIMO controller has been designed based on the filtered-X least mean square (LMS) algorithm. The controller structure includes an on-line adaptive system identification that provides the LMS controller with a reasonably accurate model of the plant. The controller is capable of tracking time-varying parameters in the plant and providing effective control. The wing model in closed loop exhibits highly damped responses at airspeeds where the open-loop responses are destructive. Simulations with the flexible wing model in a time-varying airstream show a 53% increase over its corresponding open-loop flutter airspeed. The ability of the MIMO LMS controller to suppress instabilities in a wing with abruptly changing parameters (sudden onset of flutter caused by the release of stores) has also been studied. In the examples studied, it is found that adaptation is rapid enough to successfully control flutter at accelerations in the airstream of up to 9 ft/s^2. An increase in the number of flaps provides an enhancement in the overall control authority, but results in a decrease in the convergence speed of the controller, resulting in downgraded performance. The optimum number of control flaps for the model studied is found to be four, extending along 40% of the wingspan from the tip.

Introduction

AMONG the earliest researchers in active flutter suppression, Nissim[1] developed control laws based on the concept of aerodynamic energy. Horikawa and Dowell[2] explained the wing flutter suppression problem with simple active feedback controls using a standard root-locus method. Modern control design methods in state space seem more compatible with general multi-input/multi-output (MIMO) systems, and henceforth, many techniques such as linear quadratic (LQ) optimal control theory, linear quadratic Gaussian (LQG) methodology, and eigenstructure assignment have been used.[3] Active flutter suppression laws based on LQG design and order reduction, classical design like root locus and Nyquist techniques, and other concepts have been developed at the NASA Langley Research Center and they have been implemented and successfully tested on an aeroelastically scaled wind-tunnel model in the NASA Langley Transonic Dynamic Tunnel.[4]

The adaptive scheme introduced here is of the feedforward type and essentially generates a secondary disturbance using control actuators to cancel out the primary disturbance created by the source excitation. Since the control algorithm is adaptive in nature, it is not necessary to have an accurate a priori knowledge of the plant to be controlled. For a given system and a performance index, the adaptive scheme finds a way of identifying the unknown plant and providing effective control. Also, the adaptive controller is capable of tracking changing system parameters in case the plant happens to be time varying. The wing structure in a time-varying airstream is essentially a plant with changing parameters. In addition, complex aeroelastic structures can sometimes be difficult to model accurately. Therefore, an adaptive controller with an on-line system identification process would be very suitable for active flutter suppression. However, instances of adaptive flutter control techniques are relatively few in the literature.

Adaptive signal processing was enhanced in the early 1970s with the development of the least mean square (LMS) algorithm.[5] Widrow and Stearns[6] developed an adaptive control scheme where the controller is placed in cascade with the plant and its parameters are continually updated by the LMS algorithm to minimize a certain performance criterion. Since the controller is fed with a filtered version of the excitation signal, rather than the signal itself, it is known as the filtered-X LMS algorithm. Elliott et al.[7] extended the single-channel filtered-X LMS concept and designed a multichannel (or multiple-error) feedforward LMS controller. They also discussed the application of this algorithm to active sound and vibration control where the LMS controller was used to drive secondary sources to reduce the levels of noise or vibrational fields by minimizing the sum of squares of a number of error sensor signals. Sommerfeldt and Tichy[8] studied the feasibility of such an adaptive controller to minimize the force transmitted through a two-stage vibration isolation mount.

Wing Simulation Model

The dynamic structural model of the flexible wing has been developed using the standard finite element method. The flexible wing structure is approximated by a cantilevered beam with a c.m. offset from its neutral axis. In addition to Euler–Bernoulli bending, the flexible model also incorporates torsion. Hence, a finite element model of the structure is developed that acts like a beam in bending and a rod in torsion. The elastic axis is chosen to be the neutral axis of the beam so that the bending and torsion of the straight wing structure are struc-

Received March 3, 1996; revision received Nov. 10, 1996; accepted for publication Nov. 14, 1996. Copyright © 1996 by the American Institute of Aeronautics and Astronautics, Inc. All rights reserved.

*Curators' Professor, Department of Mechanical and Aerospace Engineering and Engineering Mechanics. Associate Fellow AIAA.

†Graduate Research Assistant, Department of Mechanical and Aerospace Engineering and Engineering Mechanics.

Table 1 Geometric, structural, and aerodynamic parameters of the wing model

Variable	Description	Value
S	Span of wing	24.5 in.
c	Chord	7.0 in.
c_f/c	Ratio of flap chord to total chord	0.25
EI	Elastic modulus	2×10^4 lbf-in.^{2}
GJ	Shear modulus	1×10^3 lbf-in.^{2}
m	Mass/length	2.24×10^{-4} lbf-s^2/in.^{2}
i	Torsional moment of inertia/length	4.79×10^{-4} lbf-s^2/in.
x_c	Distance of elastic axis from leading edge	1.75 in.
x_p	Distance of c.m. from leading edge	2.2 in.
$C_{l\alpha}$	Lift coefficient/angle of attack	2π
$C_{l\delta}$	Lift coefficient/flap deflection	4.0
$C_{m\delta}$	Moment coefficient/flap deflection	-0.75
C_{hm}, $C_{h\delta}$	Hinge moment coefficients	-0.01

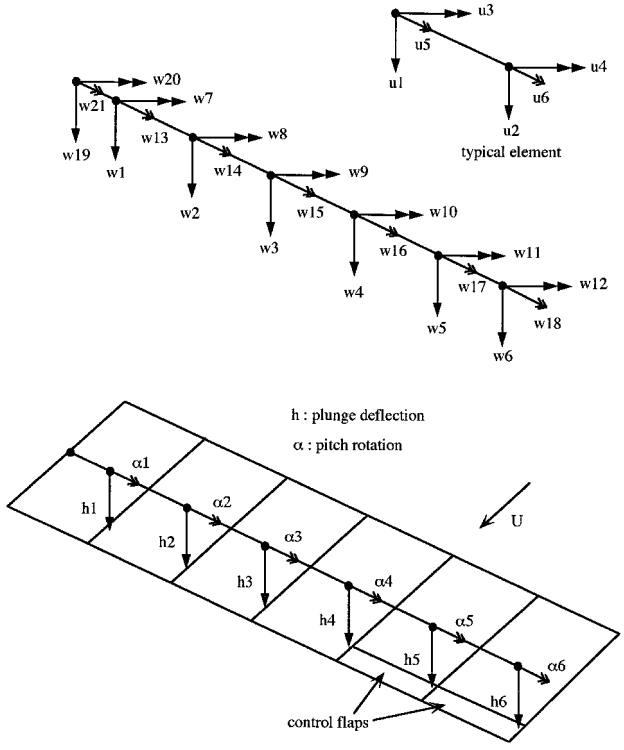

Fig. 1 Structural and aerodynamic models of the flexible wing.

turally uncoupled statically. The top diagram in Fig. 1 shows a finite element mesh for a representative wing model consisting of six elements. Each beam/rod element has six degrees of freedom; three degrees of freedom at each node. These include one translational degree of freedom, the bending displacement ($u1$, $u2$), and two rotational degrees of freedom that describe the bending slope ($u3$, $u4$) and the torsional motion about the elastic axis ($u5$, $u6$), respectively.

Aerodynamic strip theory has been utilized to account for the variation of airforces along the span of the wing. According to this theory, the airforces at any spanwise station on the wing are related to the angle of attack and/or control flap deflection only at that location. To implement the strip theory, the aerodynamic wing model has been discretized into several panels. The bottom diagram in Fig. 1 shows a representative wing model consisting of six aerodynamic panels with a finite element node at the center of each panel. This ensures full compatibility of the aerodynamic model with the finite element structural model shown in Fig. 1. It is to be noted here that although Fig. 1 shows six elements (panels), numerical simulations presented here have been performed with 10 elements (panels). For identification purposes, the panels have been numbered 1 through 10 from the wing root to the tip. Each panel has the provision of having a rigid flap at its trailing edge. If a panel has a control flap, then an additional discrete degree of freedom representing the control flap rotation δ is associated with the panel.

Following previous work,[9] the equations of motion for free vibration of the wing structure can be written as

$$[M_{ee}]\ddot{\boldsymbol{w}}_e + [K_{ee}]\boldsymbol{w}_e = 0 \tag{1}$$

where w_e are elastic degrees of freedom, and the $[M_{ee}]$ and $[K_{ee}]$ are the global mass and stiffness matrices of the wing model. A standard eigenanalysis of Eq. (1) yields n natural frequencies, $w_1, \ldots, w_n$, and their corresponding eigenvectors ϕ_i, $i = 1, \ldots, n$, n being the number of elastic degrees of freedom. The first few elastic modes are sufficient to describe the dynamical motion of the flexible wing structure, and therefore, the first m ($m < n$) eigenvectors are retained to form the modal matrix

$$[\phi] = [\phi_1 \quad \phi_2 \quad \cdots \quad \phi_m] \tag{2}$$

Time-domain unsteady aerodynamics have been used to represent the air forces on the flexible wing model. According to this theory, the lift L and the total moment M acting on each panel can be written as

$$\dot{L} + \beta_1(U/b)L = qScC_{l\alpha}\{(1 - a_1)\dot{W} + \beta_1(U/b)W\} + qScC_{l\delta}\{(1 - a_1)\dot{\delta} + \beta_1(U/b)\delta\} \tag{3}$$

$$\dot{M} + \beta_1(U/b)M = qScC_{l\alpha}b(\tfrac{1}{2} + a)\{(1 - a_1)\dot{W} + \beta_1(U/b)W\} + qSc^2C_{m\delta}\{(1 - a_1)\dot{\delta} + \beta_1(U/b)\delta\} \tag{4}$$

where U is the airspeed, q is the dynamic pressure, S is the span of the panel, c is the total chord, δ is the control flap deflection, and $C_{l\alpha}$, $C_{l\delta}$, and $C_{m\delta}$ are the appropriate aerodynamic coefficients. $b = c/2$ is the semichord, ab is the location of the elastic axis aft of the midchord, a_1 and β_1 are aerodynamic parameters ($a_1 = 0.5$ and $\beta_1 = 0.05$), and W is defined by

$$W(t) = (\dot{h}/U) + \alpha + (\tfrac{1}{2} - a)(b/U)\dot{\alpha} \tag{5}$$

where h is the plunge displacement and α is the pitch rotation. This is consistent with a first-order lag model as an approximation to the Wagner function.[10] The approximate values of the aerodynamic coefficients and other geometric and structural parameters used in the simulations have been provided in Table 1.

The equations of motion of the wing in the physical space can now be written as

$$[M_{ee}]\ddot{\boldsymbol{w}}_e + [K_{ee}]\boldsymbol{w}_e = [F_c]\underline{\boldsymbol{\delta}}_c + \boldsymbol{Q}(t) \tag{6}$$

where $[F_c]$ is the global load matrix constructed by forming the generalized forces corresponding to the global degrees of freedom, and $\underline{\boldsymbol{\delta}}_c$ is a vector of the command control inputs to the system from the adaptive controller. $\boldsymbol{Q}(t)$ is the vector of generalized aerodynamic forces and can be defined by the first-order differential equation in vector matrix form

$$\dot{\boldsymbol{Q}} + \beta_1(U/b)\boldsymbol{Q} = [A]\ddot{\boldsymbol{w}}_e + [B]\dot{\boldsymbol{w}}_e + [C]\boldsymbol{w}_e \tag{7}$$

$[A]$, $[B]$, and $[C]$ are the aerodynamic matrices resulting from Eqs. (3) and (4) for every panel. Since the first few flexible modes define the wing model dynamics, numerical integration of the equations of motion have been carried out in the reduced-order modal domain. By using the truncated modal matrix $[\phi]$, modal transformation of Eqs. (6) and (7) yields

$$[M^*]\ddot{y} + [C_s^*]\dot{y} + [K^*]y = [F^*]\underline{\boldsymbol{\delta}}_c + R(t) \tag{8}$$

$$\dot{\boldsymbol{R}} + \beta_1(U/b)\boldsymbol{R} = [A^*]\ddot{y} + [B^*]\dot{y} + [C^*]y \tag{9}$$

where $\boldsymbol{R} = \phi^T\boldsymbol{Q}$. $[M^*]$, $[K^*]$, and $[F^*]$ are the generalized mass, stiffness, and load matrices, respectively. $[C_s^*]$ represents a structural modal damping matrix, which in this investigation introduces a 2% viscous damping in all of the retained modes, and $[A^*]$, $[B^*]$, and $[C^*]$ are modal transformations of matrices $[A]$, $[B]$, and $[C]$, respectively.

By using a standard-state variable approach, Eqs. (8) and (9) are expressed as a set of first-order differential equations and then solved using a fourth-order Runge–Kutta time-integration scheme. The first 13 constraint-fixed normal modes have been used to accurately depict the dynamic behavior of the flexible wing model (frequency of the 13th mode is 156.58 Hz). The time step of integration and the sampling time of the digital controller is maintained at 0.001 s to satisfy the Nyquist sampling criteria and to account for the spread of natural frequencies in the time integration. The flexible wing model predicts a critical flutter speed of 125 ft/s at a flutter frequency of 11.72 Hz. The wing model shows a predominance of the first cantilevered bending mode and the first torsional mode in its flutter motion. The input from an output channel m of the adaptive controller to a flap is a command control rotation δ_{c_m} to the torque tube, which acts as a torsional spring connecting the flap to the main body of the wing. The hinge spring is made stiff (uncoupled frequency in control flap rotation degree-of-freedom δ is chosen to be 60 Hz) so that the response of the open-loop system is relatively unaffected by the motion of the flap.

Adaptive Control Scheme

In the following description of the MIMO adaptive controller it is assumed that the control configuration has L error signal sensors, M control actuators, and N reference input signals. A representative two-channel LMS controller has been shown in Fig. 2 for simplicity and does not depict the actual number of I/O channels of the MIMO controller used for the simulation studies. In the development of the LMS algorithm, the output of the LMS filter is assumed to be the convolution of the input data sequence to the filter with the LMS filter coefficients. As such, the LMS algorithm is developed in the context of an adaptive finite impulse response (FIR) filter.[5] If this assumption is extended to a multichannel algorithm with M outputs, then the output of the mth LMS control filter u_{m_k} can be expressed as

$$u_{m_k} = \sum_{n=1}^{N}\sum_{i=0}^{I-1} w_{mn_i}x_{n_{k-i}} \tag{10}$$

where k is the sampling time index, x_{n_k} is the nth reference input data sequence, w_{mn_i} represents the time-varying control

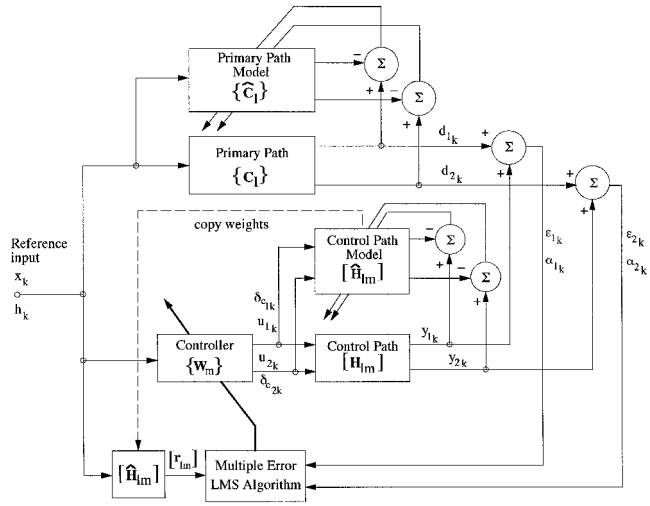

Fig. 2 Multichannel adaptive control configuration with one reference input, two error sensors, and two control actuators.

filter coefficients, and I is the number of filter coefficients. These control signals are then used to drive the M control actuators in such a way that the performance function

$$J = E\left[\sum_{l=1}^{L}\varepsilon_{l_k}^2\right] \tag{11}$$

is minimized. Here ε_{l_k} is the error signal at the lth error sensor.

The transfer function that relates the control disturbance y_{l_k} at the lth error sensor to the mth control filter output u_{m_k} is referred to as the lmth control path (or error path) transfer function and is denoted by H_{lm}. In the context of the problem at hand, this transfer function represents the combination of the mth control actuator response function, the system (wing model) transfer function between the lth error sensor and the mth control actuator, and the lth error sensor response function. If each of the control path transfer functions, H_{lm} are modeled properly by finite impulse response filters, then the response at the lth error sensor can be expressed as

$$\begin{aligned}\varepsilon_{l_k} &= d_{l_k} + y_{l_k}\\ &= d_{l_k} + \sum_{m=1}^{M}\sum_{j=0}^{J-1} h_{lm_j}u_{m_{k-j}}\\ &= d_{l_k} + \sum_{m=1}^{M}\sum_{n=1}^{N}\sum_{j=0}^{J-1}\sum_{i=0}^{I-1} h_{lm_j}w_{mn_i}x_{n_{k-j-i}}\end{aligned} \tag{12}$$

where d_{l_k} is the response to the primary excitation at the lth error sensor, which represents the disturbance to be minimized, h_{lm_j} are filter coefficients representing H_{lm} (might be time varying), and J is the number of filter coefficients. From Eq. (12) it is obvious that the adaptive control problem consists of two steps: 1) a system identification problem in determining the control path transfer coefficients h_{lm_j}, and 2) a control problem in finding the LMS control filter coefficients w_{mn_i}.

System Identification

By defining the vectors

$$\boldsymbol{H}_{lk}^T \equiv [h_{l1_0}h_{l1_1}\cdots h_{l1_{J-1}}|h_{l2_0}\cdots h_{l2_{J-1}}|\cdots|h_{lM_0}\cdots h_{lM_{J-1}}] \tag{13}$$

$$\boldsymbol{U}_k^T \equiv [u_{1_k}u_{1_{k-1}}\cdots u_{1_{k-J+1}}|u_{2_k}\cdots u_{2_{k-J+1}}|\cdots|u_{M_k}\cdots u_{M_{k-J+1}}] \tag{14}$$

the lth error signal can be represented as

$$\varepsilon_{l_k} = d_{l_k} + \boldsymbol{H}_{lk}^T\boldsymbol{U}_k \tag{15}$$

By using the assumption that the inputs to the LMS control filter x_{n_k} are correlated to the signal to be canceled d_{l_k}, the I/O relationship of the primary path can be expressed as

$$d_{l_k} = \sum_{n=1}^{N} \sum_{p=0}^{K-1} c_{ln_p} x_{n_{k-p}} \tag{16}$$

where c_{ln_p} are the coefficients of the lnth FIR filter modeling the primary path transfer function and K is the number of filter coefficients. The control filter coefficients w_{mn_i} and the control path and primary path transfer function coefficients h_{lm_j} and c_{ln_p}, respectively, might be functions of the discrete time index k. However, the subscript k has been dropped from their notations for convenience.

If the vectors in Eqs. (13) and (14) are augmented as

$$\boldsymbol{\Theta}_{lk}^T \equiv [\boldsymbol{H}_{lk}^T | \boldsymbol{C}_{lk}^T] \tag{17}$$

where

$$\boldsymbol{C}_{lk}^T \equiv [c_{l1_0} c_{l1_1} \cdots c_{l1_{K-1}} | c_{l2_0} \cdots c_{l2_{K-1}} | \cdots | c_{lN_0} \cdots c_{lN_{K-1}}] \tag{18}$$

$$\boldsymbol{\Psi}_k^T \equiv [\boldsymbol{U}_k^T | \boldsymbol{X}_k^T] \tag{19}$$

where

$$\boldsymbol{X}_k^T \equiv [x_{1_k} x_{1_{k-1}} \cdots x_{1_{k-K+1}} | x_{2_k} \cdots x_{2_{k-K+1}} | \cdots | x_{N_k} \cdots x_{N_{k-K+1}}] \tag{20}$$

the lth error signal can be conveniently expressed by

$$\varepsilon_{l_k} = \boldsymbol{\Theta}_{lk}^T \boldsymbol{\Psi}_k \tag{21}$$

In Eq. (21), ε_{l_k} and all of the entries in $\boldsymbol{\Psi}_k$ are available for measurement. The only unknown values are the primary path and control path transfer function coefficients in $\boldsymbol{\Theta}_{lk}$. If $\hat{\boldsymbol{\Theta}}_{lk}$ is an estimate of $\boldsymbol{\Theta}_{lk}$, then the estimated lth system error can be expressed as

$$\hat{\varepsilon}_{l_k} = \hat{\boldsymbol{\Theta}}_{lk}^T \boldsymbol{\Psi}_k \tag{22}$$

The estimate of the primary path and control path transfer function coefficients in $\hat{\boldsymbol{\Theta}}_{lk}$ are updated iteratively by the LMS algorithm using a steepest descent approach[5]

$$\hat{\boldsymbol{\Theta}}_{l(k+1)} = \hat{\boldsymbol{\Theta}}_{lk} + 2\mu \boldsymbol{\Psi}_k (\varepsilon_{l_k} - \hat{\varepsilon}_{l_k}) \tag{23}$$

where $(\varepsilon_{l_k} - \hat{\varepsilon}_{l_k})$ is the system identification error and μ is the adaptive gain constant regulating the speed and the stability of convergence.

System Control

The aim of this multichannel algorithm is to set up the controller in a configuration where the LMS algorithm can be readily applied to adapt its coefficients. But from Fig. 2, it is obvious that the system output error ε_{l_k} is at the control path output, not at the adaptive control filter output. If the error ε_{l_k} and the reference inputs x_{n_k} are used directly with the LMS algorithm for the control filter, the adaptive process is almost guaranteed to be unstable, or if not, to find an irrelevant solution. However, according to Elliot et al.,[7] if the LMS control filter coefficients w_{mn_i} are only slowly varying relative to the time scale of the system to be controlled, the assumption of time invariance in the filter coefficients is valid. Since the control path is estimated on-line, it is also assumed that the convergence of the system identification process takes place several times faster than that of the LMS control filter. Using these assumptions, the LMS controller and the control path transfer function are commutable and Eq. (12) can be rearranged as

$$\varepsilon_{l_k} = d_{l_k} + \sum_{m=1}^{M} \sum_{n=1}^{N} \sum_{i=0}^{I-1} w_{mn_i} r_{lmn_{k-i}} \tag{24}$$

where

$$r_{lmn_{k-i}} = \sum_{j=0}^{J-1} h_{lm_j} x_{n_{k-j-i}} \tag{25}$$

The error signal ε_{l_k} now appears at the adaptive control filter output and LMS algorithm can be used to update its coefficients. The reference input signal x_{n_k} is, however, filtered through H_{lm} before reaching the control filter, thereby generating the filtered reference r_{lmn_k}.

The optimum set of control filter coefficients w_{mn_i} required to minimize the performance function J defined by Eq. (11) is then evaluated adaptively using the gradient descent approach given by the LMS algorithm[6]

$$w_{mn_{i,k+1}} = w_{mn_{i,k}} - 2\gamma \sum_{l=1}^{L} \varepsilon_{l_k} r_{lmn_{k-i}}$$

$$m = 1, 2, \ldots, M \qquad n = 1, 2, \ldots, N \tag{26}$$

where k is the step or iteration number and γ is a convergence parameter regulating the speed and the stability of the adaptive process. For a single input/single output (SISO) system ($L = M = N = 1$), this corresponds exactly to the filtered-X LMS algorithm discussed by Widrow and Stearns.[6] It has proved to be quite robust to errors in the estimate of the control path transfer function used to generate the filtered reference input signal.[11]

Controller Configuration for the Wing Model

For the self-excited vibrations of the wing model, there is no external disturbing force that is physically measurable. Therefore, the reference exciting input x_k for the flexible wing model is chosen to be the wing-tip bending (plunge) deflection. Since the flutter in the wing model is a narrow-band phenomenon and is dominated by the flutter frequency, the choice of only one reference exciting input representing the flutter frequency is justified. The performance function to be minimized is chosen to be

$$J = E\left[\sum_{l=1}^{L} \alpha_{l_k}^2\right] \tag{27}$$

where L is the number of control flaps used for simulation and α_{l_k} is the pitch rotation at the finite element node of the panel l with a flap (the adaptive control configuration chosen for all the simulations correspond to $L = M$). Since the pitch and the plunge motions of the wing models are highly coupled, it is assumed that minimizing one would suppress the other. Besides the control flap dynamics, no other external actuator dynamics have been included in the simulation model. In a real-time implementation of the controller, the choice of an appropriate actuator is not unique. However, since the system identification is on-line, the actuator dynamics could easily be adaptively modeled in the control path as long as the actuator response function is capable of being approximated by a linear system.

Simulation Results

The wing vibration at the onset of flutter is nearly harmonic in nature. The spectral character of the plunge and the pitch disturbance signals, measured at any position on the wing, at

and beyond flutter, are narrow band and alike (i.e., the dominant peaks in both pitch and plunge disturbance signals correspond to the same frequencies). These features make the adaptive LMS controller, a MIMO extension of the filtered-X LMS algorithm, very well suited to the problem of wing flutter suppression. First, adaptation, in both system identification and control, is fast when dealing with predominantly harmonic signals. In fact, the filtered-X LMS algorithm has been shown to yield excellent results in harmonic control.[7,8] Second, the multiple-error LMS algorithm assumes that the primary disturbance signals d_{l_k} are correlated to the reference input signal x_k, so that appropriate cancellation at all existing frequencies is possible by driving the control path transfer function with suitable control outputs u_{l_k} (refer to Fig. 2).

The simulation results of the flexible wing pertain to a model made of 10 equal aerodynamic panels with control flaps on panels 7–10, the outer 40% of the wingspan, driven by the command control rotations $\underline{\delta}_{c_i}$, $i = 1, \ldots, 4$ from a four-channel LMS controller. The airspeed is varied continuously from 120 to 192 ft/s (4% below critical flutter speed to 53% above) at a rate of 9 ft/s^2. Such a case is indicative of a fairly rapid acceleration through the flutter boundary. The disturbance input is generated by the control flap on the outermost panel (panel 10), which is perturbed every 3 s to initiate the flutter motion. The sole purpose of this excitation is to simulate the effect of turbulence that might be in the airstream and that presumably initiates the flutter. It is not intended to provide training signals for the control path estimation. The on-line system identification scheme for the control path converges to a solution based on the signals that are naturally available from the wing model. Figure 3 shows the open-loop response of the wing tip. At subcritical flutter speeds, the wing shows damped decaying oscillations when excited. As the airspeed reaches critical flutter speed (125 ft/s) at 0.56 s, the oscillations grow divergent, ultimately leading to structural failure. Figure 4 shows the closed-loop response of the wing model with the controller on at all times. The system identification/controller structure adapts as the wing starts to diverge at flutter speed, but stabilizes quickly once the adaptive process converges. The controller is able to suppress flutter up to an airspeed 53% above open-loop flutter speed. This is a significant improvement over a previous investigation[9] where the performance of a SISO version of the adaptive controller, acting on the same flexible wing model, was evaluated. The SISO control configuration was able to control flutter up to an airspeed 36% above the critical flutter speed. The SISO controller drove only one flap extending along 20% of the wingspan. The MIMO control configuration has the capability of actuating multiple flaps (four used in this study) covering a total length of 40% of the wingspan. This results in a greater control authority.

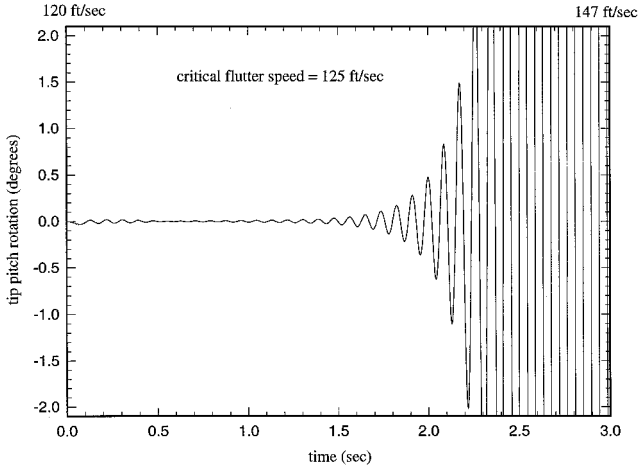

Fig. 3 Open-loop response of the flexible wing.

Figure 5 shows the time histories of two output channels of the controller that provide command control rotations to the flaps located on panels 7 and 8. The phase relations between the flap motions emphasize the fact that it is not appropriate to actuate a flap not nearly colocated with the sensor that drives it. This explains the increased performance of the MIMO controller, as compared to the SISO controller in Ref. 9. Figure 6 illustrates the on-line system identification process of one channel. It shows the time history of the actual error signal ε_{4_k} measured at the outermost panel 10 vs the corre-

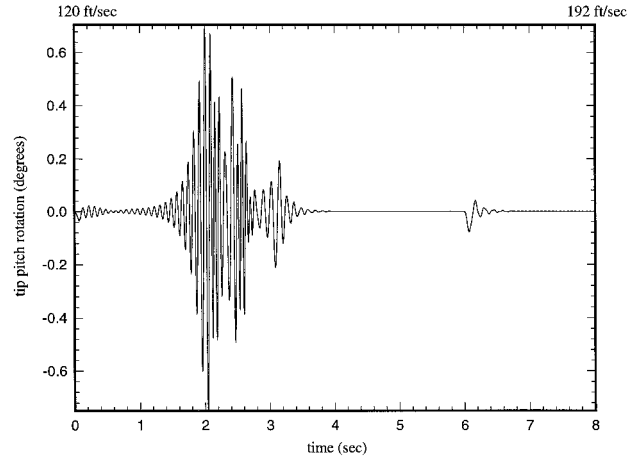

Fig. 4 Closed-loop response of the flexible wing.

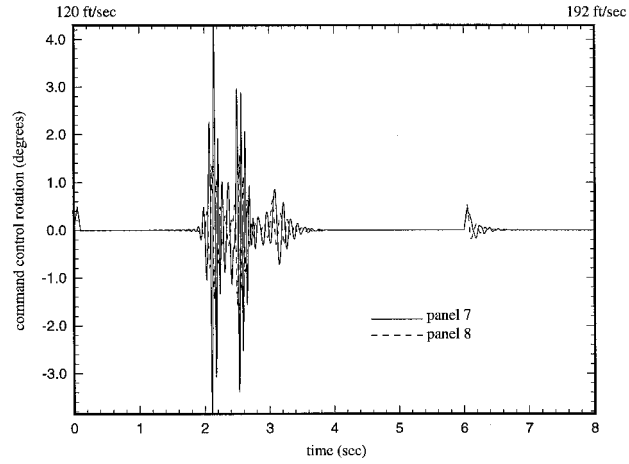

Fig. 5 Time history of the multichannel controller outputs.

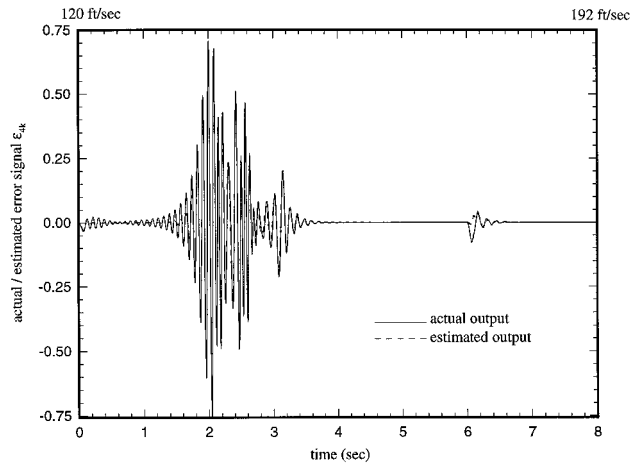

Fig. 6 System identification of a control path in the flexible wing.

sponding estimated signal formed from the combination of the primary path model and the control path model outputs. Since the signals that are available to the system identification are predominantly harmonic and not strongly persistently exciting (signals do not excite all of the possible modes within the system's bandwidth), the estimated control path model converges quickly, but probably does not converge to its true parameters.[12] However, the converged solution does minimize the estimation error and provides proper I/O relationships for the frequencies present.

Figure 7 depicts the convergence process of the adaptive LMS control filters. The filter coefficients remain virtually unaffected until the divergent motion in the wing becomes reasonably large to provide enough impetus to the adaptive process upon which they undergo a sharp rise in their values, indicating quick and forceful control action. Figure 8 illustrates the capability of the MIMO adaptive controller to suppress flutter at a speed that is well beyond the critical flutter speed. This is the result of a simulation in which no input disturbance is applied until the airspeed is 138 ft/s (10% above critical flutter speed). It demonstrates suppression of the instabilities when the first disturbance is caused well above the flutter speed. There is no prior training or adaptation. The outermost control flap in this case is perturbed every 3 s to initiate flutter upon which the controller acts forcefully to suppress the divergent motion. This can be considered as a simulation of a system that experiences a sudden change in parameters (plant change), which lowers the flutter speed below the flight speed, for example, the release of an external store. The number of taps in each of four FIR digital control filters W_m, $m = 1, \ldots 4$, used for the previous study is 45.

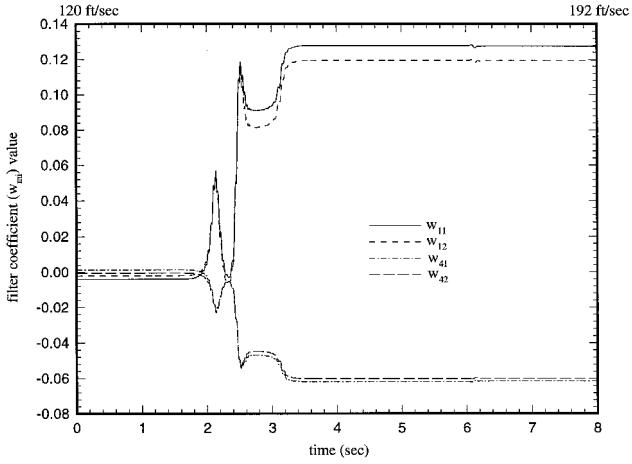

Fig. 7 Convergence of the LMS control filter coefficients.

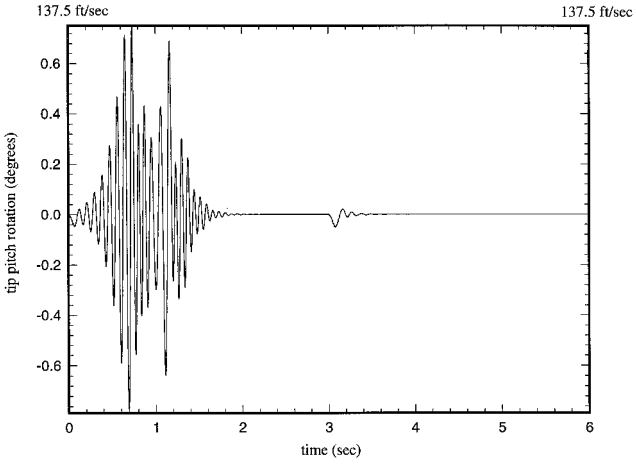

Fig. 8 Closed-loop response of the adaptively controlled flexible wing with a sudden plant change.

The adaptive MIMO LMS controller performs satisfactorily in suppressing flutter of the wing without any prior knowledge of the model. However, as is to be expected in an adaptive scheme, the performance of this control configuration is limited by the acceleration of the airstream (that is, the rate at which the plant varies). As the acceleration is increased beyond 9 ft/s^2, the controller is unable to adapt rapidly enough to successfully suppress the instability. However, the acceleration threshold value of 9 ft/s^2 for the MIMO control configuration acting on the flexible wing model is still a noticeable improvement over 7 ft/s^2, when the SISO controller acted on the same model.[9] This is achieved by the use of multiple control flaps resulting in a greater control authority for the MIMO case.

For the flexible wing model, the four output channels of the MIMO controller actuate four flaps located on panels 7–10, covering only 40% of the wingspan. Also, because of the finite span effect corrections, the aerodynamic lift and moment generated in the flexible wing because of control flap deflections drop along the span from the wing root to the tip. These two factors are responsible for reduced control authority in the flexible model when compared to a wing with flaps along the entire wingspan. The authority obviously increases with the addition of more control flaps, but it also increases the number of I/O channels in the LMS controller. For a multichannel LMS controller with L error sensors, M actuators, and a single reference input signal, the stability range for the convergence parameter γ in Eq. (26) is given by[13]

$$0 < \gamma < \frac{1}{h_{\max}^2[L \cdot M \cdot I \cdot J^2]R_{xx}(0)} \tag{28}$$

where $R_{xx}(0)$ represents the average power of the reference input signal x_k, and $h_{\max}$ represents the largest value the coefficients h_{lm_j} may assume. From the previous range it is clear that as the number of error sensors and control actuators (and, hence, the number of flaps) are added to the flexible wing model, the control algorithm must converge at a slower rate, everything else remaining equal. Therefore, though control authority increases with the addition of flaps, the convergence of the multichannel adaptive controller becomes slower. Since the flexible wing model during flutter is open-loop unstable, a slow reaction from the controller does not usually prevent the plant from being driven toward instability. According to Eq. (28), a SISO-filtered-X LMS controller has the highest convergence rate. As the number of channels in the MIMO controller (and, hence, the number of flaps) is increased from 1 through 4, an increase in the control authority is observed without sacrificing the speed of convergence significantly. However, as the number of channels exceeds four, the convergence rate of the algorithm decreases considerably, resulting in downgraded performance. No systematic method has been followed to optimize the location of these four control flaps. However, after numerical experimentation, the optimum locations were found to be on panels 7–10.

Summary

The objective of this study was to determine the feasibility of using an adaptive feedforward MIMO control structure for active flutter suppression of a flexible wing. For numerical simulation purposes, a multi-degree-of-freedom finite element structural model of a flexible wing has been constructed. The control actuators for this model were four flaps attached to the trailing edge of the wing and covering a total length of 40% of the wingspan from the tip. An adaptive feedforward MIMO controller has been developed based on the filtered-X LMS algorithm. The controller structure also included an on-line system identification scheme that provided the LMS controller

with a reasonably accurate model of the plant. In numerical simulations, the effectiveness of the adaptive controller acting on the wing model has been examined with the airspeed varying from a subcritical flutter speed to the maximum closed-loop airspeed the system could sustain (63% above flutter). The adaptive controller was also successful in suppressing instabilities arising because of abruptly changing plant parameters (up to 10% above flutter). The MIMO control configuration, however, failed to provide flutter suppression during very rapid accelerations of the airstream (above 9 ft/s^2 for the flexible wing model) because of insufficient control authority and the inability of the adaptive process to cope with such rapid changes. The control authority could be boosted by the addition of more flaps to the flexible wing model. However, as the number of control flaps was increased, the number of I/O channels in the LMS controller increased, resulting in a slower convergence of the adaptive process. Numerical experimentation found that four control flaps on the outer 40% of the wingspan driven by a four-channel LMS controller yielded the best results for the flexible wing model.

Acknowledgment

The authors thank W. H. Tranter of the Electrical Engineering Department at the University of Missouri–Rolla for his valuable advice in adaptive signal processing.

References

[1]Nissim, E., "Flutter Suppression Using Active Control Based on the Concept of Aerodynamic Energy," NASA TN-D-6199, March 1971.

[2]Horikawa, H., and Dowell, E. H., "An Elementary Explanation of the Flutter Mechanism with Active Feedback Controls," *Journal of Aircraft*, Vol. 16, No. 4, 1979, pp. 225–232.

[3]Garrard, W. L., and Liebst, B. S., "Active Flutter Suppression Using Eigenspace and Linear Quadratic Design Techniques," *Journal of Guidance, Control, and Dynamics*, Vol. 8, No. 3, 1985, pp. 304–311.

[4]Perry, B., Mukhopadhayay, V., Hoadley, S., Houck, J., Buttrill, C., and Cole, S., "Digital Flutter Suppression System Investigations for the Active Flexible Wing Wind-Tunnel Model," *Proceedings of the AIAA/ASME/ASCE/AHS/ASC 31st Structures, Structural Dynamics, and Materials Conference* (Long Beach, CA), AIAA, Washington, DC, 1990, pp. 1571–1581.

[5]Widrow, B., "Adaptive Filters," *Aspects of Network and System Theory*, edited by R. E. Kalman and N. De Claris, Holt, Rinehart, and Winston, Philadelphia, PA, 1970, pp. 563–587.

[6]Widrow, B., and Stearns, S. D., *Adaptive Signal Processing*, Prentice–Hall, Englewood Cliffs, NJ, 1985.

[7]Elliott, S. J., Stothers, I. M., and Nelson, P. A., "A Multiple Error LMS Algorithm and Its Application to the Active Control of Sound and Vibration," *IEEE Transactions on Acoustics, Speech and Signal Processing*, ASSP-35, No. 10, Oct. 1987, pp. 1423–1434.

[8]Sommerfeldt, S. D., and Tichy, J., "Adaptive Control of a Two-Stage Vibration Isolation Mount," *Journal of the Acoustical Society of America*, Vol. 88, No. 2, 1990, pp. 938–944.

[9]Danda Roy, I., and Eversman, W., "Adaptive Flutter Suppression of an Unswept Wing," *Journal of Aircraft*, Vol. 33, No. 4, 1996, pp. 775–783.

[10]Bislinghoff, L. J., Ashley, H., and Halfman, R. L., *Aeroelasticity*, Addison–Wesley, Reading, MA, 1955.

[11]Boucher, C. C., Elliott, S. J., and Nelson, P. A., "Effect of Errors in the Plant Model on the Performance of Algorithms for Adaptive Feedforward Control," *IEEE Proceedings-F, Special Issue on Adaptive Filters: Theory and Practice*, Vol. 138, No. 4, 1991, pp. 313–319.

[12]Goodin, G. C., and Sin, K. S., *Adaptive Filtering, Prediction and Control*, Prentice–Hall, Englewood Cliffs, NJ, 1984.

[13]Sommerfeldt, S. D., "Adaptive Vibration Control of Vibration Isolation Mounts, Using an LMS-Based Control Algorithm," Ph.D. Dissertation, Pennsylvania State Univ., University Park, PA, 1989.